

ManipDreamer3D : Synthesizing Plausible Robotic Manipulation Video with Occupancy-aware 3D Trajectory

Ying Li^{1,3}, Xiaobao Wei^{1,3}, Xiaowei Chi^{*2}, Yuming Li¹, Zhongyu Zhao¹, Hao Wang¹, Ningning Ma³, Ming Lu¹, Shanghang Zhang^{† 1}

¹State Key Laboratory of Multimedia Information Processing, School of Computer Science, Peking University

²Hong Kong University of Science and Technology ³Autonomous Driving Development, NIO

myendless@stu.pku.edu.cn

Abstract

Data scarcity continues to be a major challenge in the field of robotic manipulation. Although diffusion models provide a promising solution for generating robotic manipulation videos, existing methods largely depend on 2D trajectories, which inherently face issues with 3D spatial ambiguity. In this work, we present a novel framework named ManipDreamer3D for generating plausible 3D-aware robotic manipulation videos from the input image and the text instruction. Our method combines 3D trajectory planning with a reconstructed 3D occupancy map created from a third-person perspective, along with a novel trajectory-to-video diffusion model. Specifically, ManipDreamer3D first reconstructs the 3D occupancy representation from the input image and then computes an optimized 3D end-effector trajectory, minimizing path length while avoiding collisions. Next, we employ a latent editing technique to create video sequences from the initial image latent and the optimized 3D trajectory. This process conditions our specially trained trajectory-to-video diffusion model to produce robotic pick-and-place videos. Our method generates robotic videos with autonomously planned plausible 3D trajectories, significantly reducing human intervention requirements. Experimental results demonstrate superior visual quality compared to existing methods.

Introduction

Collecting real-world robot manipulation demonstrations is often time-consuming, labor-intensive, and constrained by hardware limitations (Park et al. 2024; An et al. 2025). These challenges hinder the scalability of robotic policy learning, where large and diverse datasets are critical for achieving robust generalization (Schmidt et al. 2018; Xu and Mannor 2012). Generating realistic demonstrations with safe and short trajectories becomes particularly important (Ding et al. 2020; Hanselmann et al. 2022), as it can reduce the dependency on extensive physical data collection while providing high-quality supervision for an effective robot policy model.

Recent works have sought to expand real-world robot manipulation datasets by replaying recorded trajectories with diverse visual augmentations, such as altering objects, robot embodiments, textures, backgrounds, distractors, lighting conditions, and camera viewpoints (Mandi et al. 2022; Chen

et al. 2023; Fang et al. 2025; Yang et al. 2025a; Huang et al. 2024a; Wei et al. 2024). Beyond augmentation-based replay, Re³Sim (Han et al. 2025) reconstructs realistic scenes in simulation to synthesize plausible manipulation demonstrations. ORV (Yang et al. 2025b) introduces a different strategy, using 4D semantic occupancy as an intermediate representation to generate realistic videos from either real-world or simulated data. Improving synthesis fidelity is not sufficient for robotics. Modeling the robotic actions plays a critical role in producing realistic manipulation videos. This&That (Wang et al. 2025a) conditions generation on object and target gestures, whereas RoboMaster (Fu et al. 2025) jointly models both robot and object trajectories to guide the generation process.

While these approaches have generated promising robotic videos, several limitations remain. First, existing methods often overlook that robotic actions are planned in a 3D space. As a result, the generated videos may contain trajectories that violate physical constraints, lack collision avoidance, motion safety, or execution efficiency. These methods still rely heavily on manual object selection or annotation (Yang et al. 2025b; Wang et al. 2025a; Fu et al. 2025). Second, the generated scenes fail to maintain geometric and physical consistency with real-world environments (Wang et al. 2025a; Zhou et al. 2024; Li et al. 2025). Even when the generated 2D videos exhibit promising perceptual quality, inaccuracies in object size, placement, or contact state can lead to unrealistic 3D interactions, such as incorrect grasping pose. These issues significantly limit the applicability of such videos for training generalizable robotic policies.

To overcome these limitations, we propose ManipDreamer3D, a novel method to automatically generate plausible robotic manipulation videos given a third-view observation image along with an instruction. The key idea is to first reconstruct a 3D occupancy representation of the scene and plan a physically valid, short manipulation trajectory from the robot end-effector to the manipulated object, and to the destination. We then synthesize the corresponding video conditioned on this planned trajectory. The overall functionality of our method is shown in Fig. 1.

Specifically, we first construct the 3D occupancy from third-view observations. Second, we extract 3D trajectories for the end-effector and the target object, spanning from the initiation state to task completion, the trajectories are then post-processed according to a predefined velocity profile. Fi-

^{*}Project Leader

[†]Corresponding Author

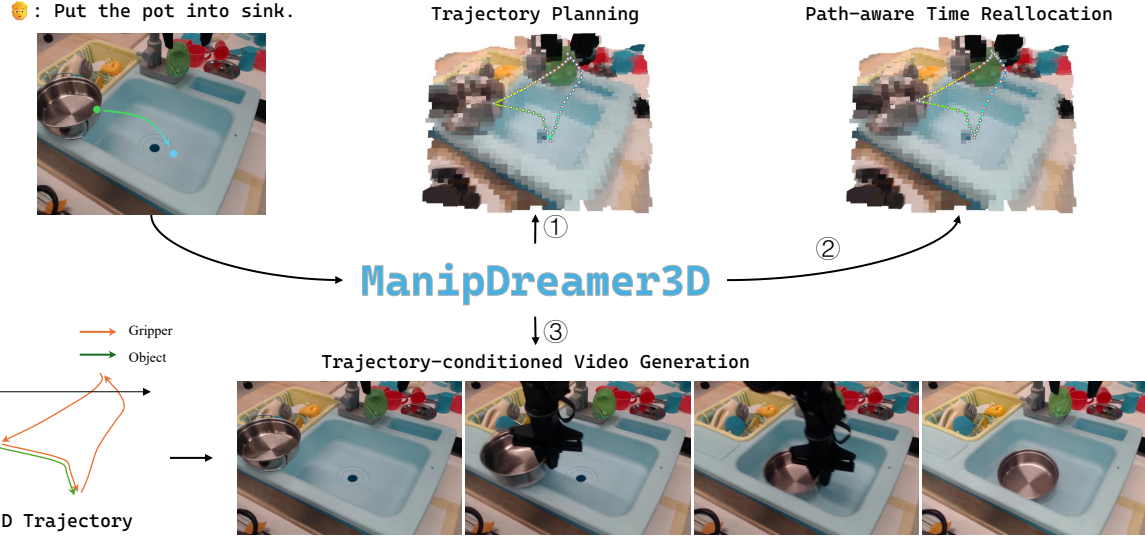


Figure 1: **Overview of our proposed method ManipDreamer3D**. Given a user-specified third-view image, an instruction, and a gesture, ManipDreamer3D first constructs an occupancy grid and initializes a feasible trajectory within the grid space for optimization. The method then reallocates time based on the sub-trajectory path lengths and a predefined velocity profile. Finally, ManipDreamer3D synthesizes the output video conditioned on the trajectories of both the robot end-effector and the object.

nally, we employ an efficient diffusion-based latent editing strategy that transforms the initial image latent into a temporally coherent video latent, which is then concatenated with noised video latent to serve as guidance. This method introduces no additional parameters beyond the original diffusion model. In conclusion, our key contributions are threefold.

- We propose a novel occupancy-aware 3D trajectory planner that yields physically plausible, collision-free, and length-efficient end-effector trajectories.
- We introduce a simple and efficient trajectory conditioned video generation scheme, which seamlessly plugs into diffusion-based models without extra parameters or auxiliary modules.
- Our comprehensive experiments across diverse manipulation scenarios demonstrate that ManipDreamer3D achieves SOTA performance in robotic trajectory-conditioned video generation, outperforming existing methods across multiple video quality metrics while maintaining precise trajectory control.

Related Works

Robotic Trajectory Planning

Trajectory planning is a critical component in robotics, particularly in vision-language navigation (VLN) (Zhang et al. 2024; Wei et al. 2025) and vision-language-action (VLA) tasks (Kim et al. 2024). A common paradigm of path planning in VLN involves constructing a global representation of the environment to support subsequent path planning. For instance, (Wang et al. 2025c) proposes a method that samples path proposals via a random walk strategy and scores them using a multi-modal transformer within a global 3D semantic map. Alternatively, some studies leverage large language

models (LLMs) for reasoning and planning based on human instructions and visual observations. NavGPT (Zhou, Hong, and Wu 2024) utilizes a supportive interaction and memory tracking framework, while (Chen et al. 2024) employs a global topological node map to enhance spatial reasoning for LLMs.

In contrast to VLN’s global planning focus, the VLA field prioritizes sequential action prediction in an implicit target-approaching manner, often generating short-term action chunks rather than explicit global paths (Zitkovich et al. 2023; Kim et al. 2024; Black et al. 2024). For instance, Open-VLA processes the current observation to output the next 16 actions chunk (15 Hz control) or 8 actions chunk (5 Hz control) in relative coordinates, while π_0 (Black et al. 2024) employs a 50-step action horizon. These predicted actions are subsequently refined into executable trajectories by low-level controllers using inverse-dynamics systems, typically through numerical algorithms like RRT and CHOMP.

Unlike VLA models that predict conditional action distributions based on observation history and robot states, robotic manipulation video generation requires globally optimal paths that are both efficient and physically plausible. To address this, we propose planning complete 3D trajectories in occupancy space, optimized using a CHOMP-inspired method. We detail this trajectory planning approach in the first part of our method.

Trajectory Controlled Video Generation

Recent advances in motion-controlled video generation using diffusion models have demonstrated remarkable progress. TrailBlazer (Ma, Lewis, and Kleijn 2024) introduces sparse keyframe bounding boxes to guide object motion. DragNUWA (Yin et al. 2023) enhances motion robustness through

Method	Keypoint Control	Full Trajectory Control	Affordance Control
This&That	✓	✗	✗
RoboMaster	✓	✓	✗
ManipDreamer3D	✓	✓	✓

Table 1: **Control capabilities of existing methods.** Ours ManipDreamer3D provides the most fine-grained control by jointly supporting keypoint, full-trajectory, and affordance control.

trajectory maps and integrates text, image, and trajectory information via multi-scale fusion in UNet layers. DragAnything (Wu et al. 2024) employs both 2D Gaussian maps and entity feature maps extracted using a pretrained text-to-image model for generation guidance. MotionCtrl (Wang et al. 2024) unifies camera and object motion control through two dedicated modules: Camera Motion Control Module (CMCM) and an Object Motion Control Module (OMCM). A recent work, DaS (Gu et al. 2025), proposes a unified 3D-tracking representation that models both camera and object motion in a unified manner by tracking 3D point movements in world coordinates.

Recent work extends these methods to robotic video generation, where motion primarily comes from the robot arm and manipulated objects, as camera position is typically fixed. The core challenge lies in how to efficiently model robot and object motion. This&That (Wang et al. 2025a) uses a 2D Gaussian map video, placing one Gaussian at the object’s initial position (at grasping time) and another at its target (at placement time), then guides generation via a Control-Net. RoboMaster (Fu et al. 2025) divides the manipulation process into three phases based on different moving agents, edits latents according to the trajectory, and injects the latents using a spatial-temporal convolution injection module at each DiT block.

Method

Problem Formulation

Given a single third-view observation image $I_0 \in \mathbb{R}^{3 \times H \times W}$ and corresponding instruction t , our goal is to generate a 3D-aware robot manipulation video. The pipeline consists of four main components: 1) We first construct a 3D occupancy map $O \in \mathbb{R}^{h \times w \times d}$ representing scene geometry. This discrete volumetric representation captures the spatial distribution of objects in the manipulation environment. 2) Using the occupancy map, we plan an initial 3D trajectory $P_{init}^3 \in \mathbb{R}^{N \times 3}$ via the A^* algorithm and optimize it through gradient descent to obtain the final trajectory P^3 . The process generates both the object trajectory P_o^3 and the end-effector trajectory P_g^3 . 3) These 3D trajectories are projected to 2D guidance maps $G \in \mathbb{R}^{N \times 3 \times H \times W}$. 4) The output video $V \in \mathbb{R}^{N \times 3 \times H \times W}$ is generated through our latent-editing control method. Different from existing trajectory-control robotic video generation methods (Wang et al. 2025a; Fu et al. 2025), our method offers the most fine-grained control, as in Tab. 1 and showcases in Fig. 7.

Occupancy-aware path planning

3D Occupancy Map Reconstruction To enable effective robot motion planning, we first establish an accurate 3D representation of the scene. We decide to use occupancy to represent the matters in the scene, as it largely reduces the points in the scene and provides an effective scene representation to plan a path. We apply three steps to construct an occupancy grid given a single-view observation. Firstly, we leverage VGGT’s (Wang et al. 2025b) 3D scene understanding capabilities to generate an initial point cloud in camera coordinates. However, this raw point cloud exhibits sparsity in regions where adjacent image planes correspond to discontinuous 3D surfaces. To address this limitation, we employ a neural surface reconstruction technique (Huang et al. 2023) to generate a dense mesh representation. From this reconstructed surface, we uniformly resample points to create a more complete point cloud. Finally, we discretize the 3D space by converting the processed point cloud into a $64 \times 64 \times 64$ occupancy grid, where each voxel indicates the presence or absence of matter. Fig. 2 (a) illustrates this multi-stage 3D reconstruction pipeline.

Optimal Trajectory Planning We propose a two-stage method to find a locally optimal manipulation path in 3D occupancy space. First, we generate an initial trajectory using the A^* algorithm applied three times for different stages:

- **Approaching stage.** Plan a path from the end-effector’s 3D position to the object’s position.
- **Manipulating stage.** Move while grasping the object from its initial position to the target position.
- **Back-idle stage.** Return the end effector to the start position.

These sub-trajectories P_1, P_2, P_3 are concatenated to form the initial trajectory $P_{init}^3 = P_1^3 \parallel P_2^3 \parallel P_3^3$, where \parallel denotes concatenation. While A^* provides a heuristic solution, the trajectory is further optimized for safety and smoothness.

Inspired by the widely used CHOMP algorithm, we optimize these sub-trajectories respectively with multiple objectives to find plausible, short, and smooth paths as shown in Fig. 2(b). Note the i th point in a given path P^3 as \mathbf{p}_i , the objectives are formulated as follows.

Collision Loss. A signed distance field (SDF) is constructed to represent the field of distance toward the static background of the scene, and a safe distance hyperparameter is adapted.

$$\mathcal{L}_{col} = \sum_{i=1}^N (SDF(\mathbf{p}_i))$$

Path Length Loss. This target aims to minimize the path length, ensuring the effectiveness of robot manipulation.

$$\mathcal{L}_{len} = \sum_{i=1}^{N-1} \|\mathbf{p}_i - \mathbf{p}_{i+1}\|^2$$

Smoothness Loss. Smooth loss includes two parts, an acceleration loss and a curvature loss. This loss avoids sharp

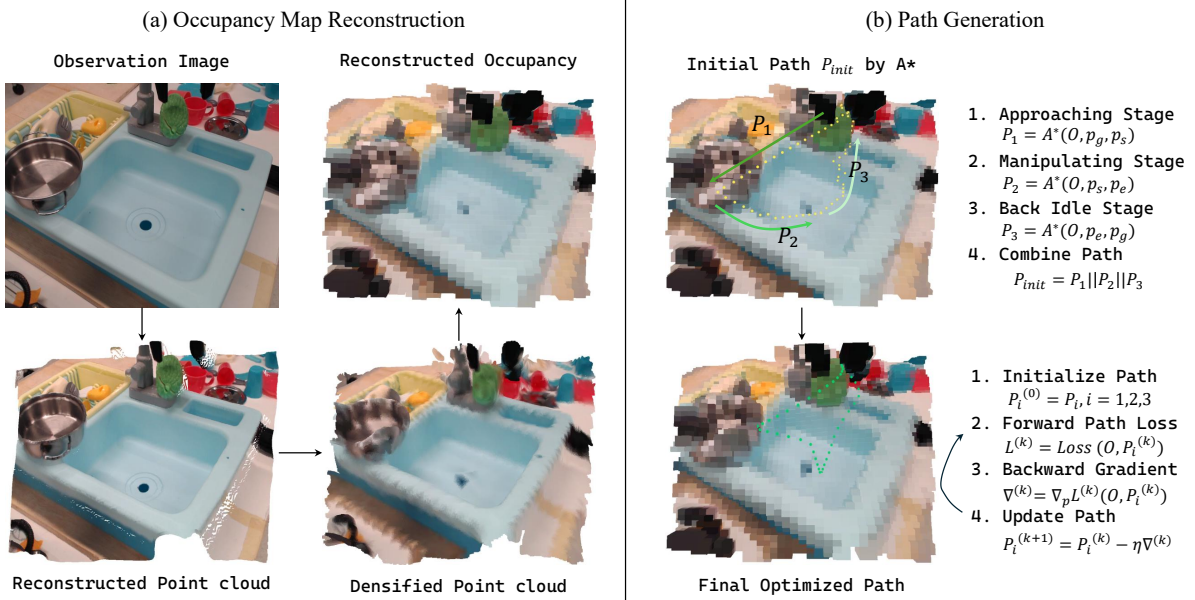


Figure 2: **The occupancy construction and trajectory pipeline.** (a) In the occupancy reconstruction process, we first estimate and densify the point cloud, then extract an occupancy out of the densified point cloud. (b) The procedure of path planning in occupancy. We first generate 3 initial sub-trajectories using A^* , and then each sub-trajectory is then optimized with gradient descent. We formulate the optimization process of a given path P here.

acceleration or direction changes of robot end effector. These two objectives are formulated as below:

$$\mathcal{L}_{acc} = \frac{1}{2} \sum_{i=1}^{N-2} \|\mathbf{p}_{i+2} - 2\mathbf{p}_{i+1} + \mathbf{p}_i\|^2$$

$$\mathcal{L}_{curv} = \frac{1}{2} \sum_{i=1}^{N-2} \left(\frac{\|\mathbf{v}_i \times \mathbf{a}_i\|^2}{\|\mathbf{v}_i^3\|^2} \right)$$

where $\mathbf{v}_i = \mathbf{p}_{i+1} - \mathbf{p}_i$ is velocity of each point, $\mathbf{a}_i = \mathbf{p}_{i+2} - 2\mathbf{p}_{i+1} + \mathbf{p}_i$ is the acceleration,

$\epsilon = 1e^{-6}$ is a small constant for numerical stability and \times denotes the cross product. Note that the start and end are specially treated and are not optimized, therefore keeping their original position. We optimize the point group P^3 to minimize the following objective using Adam optimizer and a learning rate of 0.1 for a fixed number of iterations and finally obtain P_{opt}^3 :

$$\min_{P^3} (\omega_{len}\mathcal{L}_{len} + \omega_{curv}\mathcal{L}_{curv} + \omega_{acc}\mathcal{L}_{acc} + \omega_{col}\mathcal{L}_{col})$$

After the optimization process, we obtain optimized sub-trajectories $P_i^3, i = 1, 2, 3$ that are plausible, as short and more safe in their path shape. However, due to the ignorance of the above objectives towards the mechanic nature of robot, the speed distribution of the above points follows poorly with real robots, which typically first accelerate and then decelerate within each sub-trajectory.

Path-aware Time Reallocation To adjust the robot's speed throughout the manipulation process according to a predefined velocity profile, we propose a post-processing method

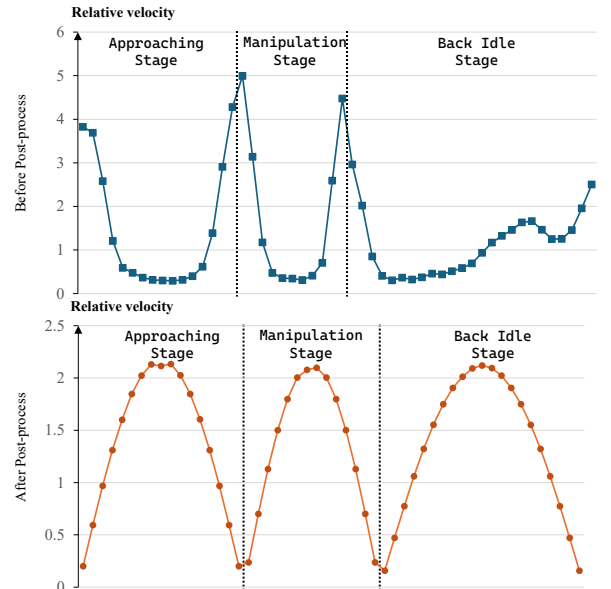


Figure 3: **Distribution of velocity before and after path-aware time reallocation of one example.**

that redistributes trajectory points based on path length and desired speed characteristics. First, the number of points in each sub-trajectory is reassigned proportionally to its arc length. Then, each point is repositioned along the path via interpolation between the two nearest original points, ensuring the resulting spatial distribution matches the intended

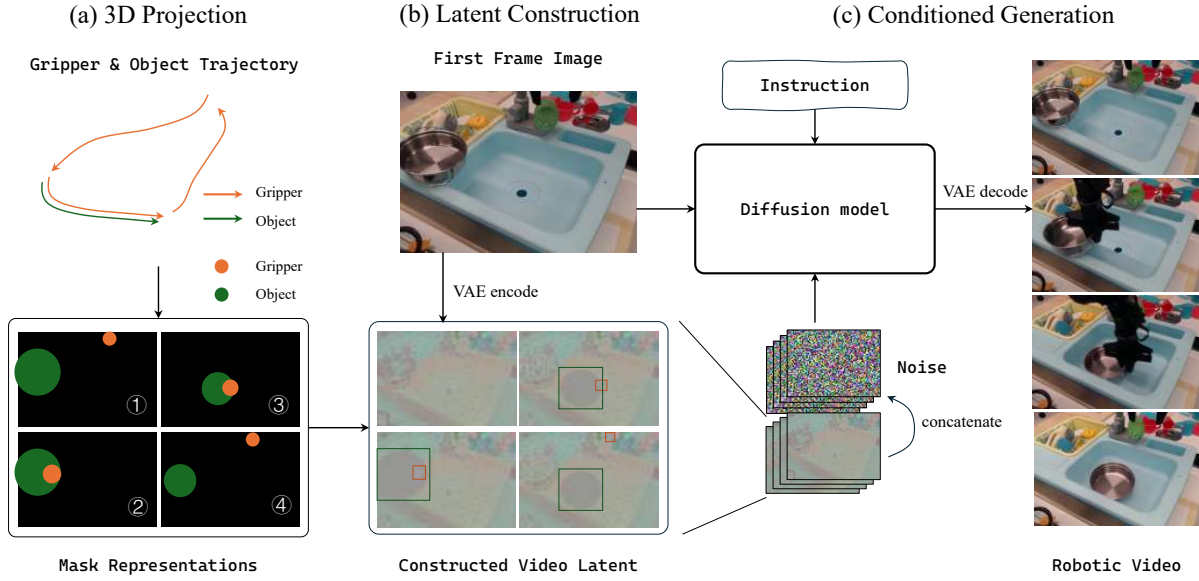


Figure 4: **The conditioned Video generation pipeline.** (a) We use a 3D-to-2D projection to create masks that represent the position and distance of object or gripper in each frame, we draw the mask of object and gripper in the same mask for clarity. (b) We apply a latent editing method using the first frame latent and the corresponding masks to create a video latent. (c) We use the constructed video latent to guide the generation of robotic videos.

velocity profile. We use sine wave as our default velocity profile for each sub-trajectory.

As shown in Fig. 3, the velocity distribution of the original trajectory exhibits inconsistencies with physics rules, whereas the recalculated trajectory after post-processing adheres more closely to physically realistic motion constraints. This realignment results in a velocity profile that is both smoother and more applicable to real-world execution.

3D Trajectory Data Curation

To train our diffusion model for generating videos from 3D robotic manipulation demonstrations, we developed a comprehensive data curation pipeline that processes three core components: 3D point cloud reconstruction of the scene to map 2D video pixels to corresponding consistent 3D coordinates, 3D robot end-effector trajectory tracking, and object detection and segmentation.

3D Scene Reconstruction. We first generate temporally consistent point clouds estimates for each frame of the third-view 2D video by processing the entire sequence with a VGGT model (Wang et al. 2025b). This produces a group of unified 3D point maps of the scene along with estimated camera parameters.

End-Effector Localization. Accurately localizing the 3D position of the robotic end-effector is challenging due to its dynamic motion and lack of fixed reference points. To address this, we employ a fine-tuned YOLO model (Yaseen 2024) specifically trained to detect the gripper fingers. The 2D centers of the detected bounding boxes are then mapped to their corresponding 3D coordinates, and the midpoint between these two positions is used as the representative 3D location of the end-effector.

Object Detection and Segmentation. We first identify the grasping initiation moment—when the gripper is about to contact the target object. Following This&That (Wang et al. 2025a), we use the gripper’s center point at this moment as an initial 2D indication of the object’s position. We then leverage Qwen-VL (Bai et al. 2023) for visual grounding, using a prompt that incorporates both the estimated position and the object name (parsed from the instruction via an LLM). Finally, we apply SAM (Kirillov et al. 2023) to generate precise object masks based on the position estimate and the resulting bounding box.

This multi-stage approach ensures high-fidelity 3D trajectory capture for both the robotic arm and the manipulated object, forming a critical foundation for training our video generation model.

Trajectory-Guided Video Synthesis

3D-to-2D Trajectory Representation Our framework transforms 3D manipulation trajectories into a compact 2D latent representation that effectively guides video synthesis. As shown in Fig. 4, the representation consists of three key components: (1) first-frame latent encoding, (2) dynamic object and end-effector projection, and (3) temporal latent construction.

Latent Editing Preparation. We initialize our representation by extracting the latent code of the first video frame using the video diffusion model’s variational autoencoder. Following RoboMaster (Fu et al. 2025), we employ pooled latent vectors to represent key scene elements: For the manipulated object, we interpolate its mask to match the latent spatial dimensions and compute the mean-pooled latent vector within the masked region. For the end-effector, we generate two dis-

Table 2: Common video metric results of our ManipDreamer3D SVD version, DiT version, and baselines.

Method		Video Quality			Trajectory Accuracy	
		FVD ↓	PSNR ↑	SSIM ↑	TrajError _{robot} ↓	TrajError _{obj} ↓
SVD-based	DragAnything	158.42	21.13	0.792	18.97	27.41
	This&That	148.69	20.93	0.758	62.07	37.12
	ManipDreamer3D(SVD)	143.33	22.75	0.807	17.40	18.77
DiT-based	RoboMaster	147.31	21.55	0.803	16.47	24.16
	ManipDreamer3D(DiT)	93.98	23.64	0.847	15.38	16.59

Table 3: The VBench metric results of our ManipDreamer3D SVD version, DiT version, and baselines.

Method		Aesthetic Quality ↑	Imaging Quality ↑	Temporal Flickering ↑	Motion Smoothness ↑	Subject Consistency ↑	background Consistency ↑
SVD-based	DragAnything	49.53	67.15	97.83	98.25	93.01	95.14
	This&That	57.27	70.09	97.20	97.91	94.43	95.45
	ManipDreamer3D(SVD)	52.46	69.24	97.98	98.47	95.39	96.57
DiT-based	RoboMaster	50.32	67.49	98.27	98.81	93.55	95.40
	ManipDreamer3D(DiT)	51.44	68.65	98.18	98.70	94.38	95.87

tinct predefined latent vectors representing open and closed states of the gripper through similar pooling operations.

3D-to-2D Projection. The projection process involves three computational steps: *Distance Estimation*: We establish the object’s depth by assuming constant camera-object distance during grasping, using the end-effector’s known 3D trajectory as a reference to estimate the change of object distance. *Geometric Abstraction*: Objects and gripper are modeled as spheres with a radius equal to the length of the longer edge of their bounding box, while the end-effector uses a predefined fixed small radius. *Perspective Projection*: We compute 2D circle projections from their 3D sphere for both object and end-effector using standard perspective projection equations.

Temporal Latent Construction. The dynamic representation is constructed in the following way: For the first frame, we simply maintain the original first-frame latent to keep the initial spatial and element representation. For the following frames, sequentially overlay the object and end-effector by filling masked regions with their corresponding pooled latent vectors. Note that we select open/closed end-effector vectors based on the gripper state here.

This representation efficiently encodes both spatial and temporal aspects of the manipulation trajectory while maintaining compatibility with the diffusion model’s architecture. The experimental results in the Experiments section demonstrate its effectiveness in guiding realistic video synthesis.

Latent-Editing Video Generation Unlike previous trajectory-conditioned methods that rely on additional ControlNet (Wang et al. 2025a) or injection modules (Fu et al. 2025) to bridge trajectory conditions with video features, our approach directly concatenates the constructed latent with the noisy video latent along the channel dimension, replacing the traditional static first-frame latent condition with a dynamic latent condition to guide the normal latent denoising process.

For UNet-based models such as SVD, where the VAE

performs only spatial compression, the constructed latent can be directly fed into the model. However, for DiT-based architectures like CogVideoX-5B (Yang et al. 2024), which uses a VAE that employs a $4\times$ temporal compression aside from spatial compression, we align the temporal dimension simply by applying a two-layer $2\times$ average pooling operation to the latent sequence.

This latent-editing strategy offers two key advantages: it maintains the original diffusion model framework by simply replacing the repeated first-frame latent with our dynamically edited version, introducing no additional parameters. Furthermore, by using the first-frame latent as the editing base, we minimize distribution shift while preserving the model’s inherent conditioning mechanism.

Experiments

Experiment Setups

Model and data details. For the data part, we train our models on the bridge V1 and bridge V2 datasets. After our curation pipeline, we finally acquired 8.7k valid episodes. Then we randomly select 90% of the examples as the training set and the rest for test usage. We implement our condition video generation method based on both pretrained stable-video-diffusion model (Blattmann et al. 2023) and CogVideoX-5B (Yang et al. 2024), we denote these two versions of our model as ManipDreamer3D (SVD) and ManipDreamer3D (DiT) respectively. The ManipDreamer3D (SVD) is trained using AdamW Optimizer on 8 NVIDIA A800 GPUs, with a learning rate of 1×10^{-5} for 50000 steps, and at inference, we use 25 inference DDIM steps. The ManipDreamer3D (DiT) model is trained using AdamW Optimizer on 8 NVIDIA A800 GPUS, with a learning rate of 2×10^{-5} for 30k steps, and at inference, we use 50 inference DDIM steps.

Metrics. To evaluate the quality of generated videos, we use common video qualities including FVD (Unterthiner et al. 2018), SSIM (Wang et al. 2004), and PSNR (Hore and Ziou 2010), as well as VBench (Huang et al. 2024b) metrics. Aside

from that, we also evaluate our model with trajectory error, which reveals how well the model follows the condition. Following (Fu et al. 2025), we evaluated this metric for the robot end-effector and the target object, respectively.

Video Quality Results

The quantitative comparisons of video generation quality are presented in Tab. 2 and Tab. 3. Our **ManipDreamer3D** demonstrates superior performance across both evaluation frameworks.

In common video metrics (Tab. 2), our SVD variant achieves best-in-class scores with FVD (143.33), PSNR (22.75), and SSIM (0.807), while significantly reducing trajectory errors (17.40 for robot, 18.77 for object) compared to SVD-based competitors including DragAnything (Wu et al. 2024) and This&That (Wang et al. 2025a). The DiT version further elevates performance, attaining 93.98 FVD and 0.847 SSIM with notably precise trajectory adherence (15.38 robot, 16.59 object error).

The trajectory accuracy advantage stems from our gripper-object collaborative representation design. While This&That relies on ambiguous two-key-gesture control and DragAnything operates at the whole-entity movement level, lacking end-effector precision, our method explicitly models the spatial position of both gripper and object throughout the interaction. RoboMaster, which uses the same DiT backbone, implicitly models the position of the end-effector during interaction, underperforms in trajectory accuracy.

VBench evaluation (Tab. 3) reveals our method’s balanced strengths: the SVD model leads in temporal stability (97.98 flickering score) and consistency metrics (95.39 subject, 96.57 background), while the DiT variant maintains competitive Imaging quality (68.65) with robust motion handling (98.70 smoothness). These results collectively validate our approach’s effectiveness in both visual quality and trajectory fidelity. We also visualize some of the same examples generated by our ManipDreamer3D based on SVD, and This&That are shown in Fig. 5. As shown in the figure, our model keeps the original shape of the original objects, while This&That suffers from object deformation. Fig. 5 presents a side-by-side comparison of manipulation sequences generated by our SVD-based ManipDreamer3D and This&That. The visual results demonstrate our method’s superior ability to maintain object structural integrity throughout the manipulation process, while This&That suffers from progressive object deformation that deviates from the original geometry. This qualitative advantage aligns with our quantitative metrics, showing better visual quality.

Key Components Analysis

The impact of trajectory optimization To evaluate the impact of trajectory optimization, we compare videos generated using initial path P_{init}^3 and optimized path P_{opt}^3 from our path planning method. As shown in Fig. 6, the P_{opt}^3 trajectory safely avoids the sink edge by moving upward, while P_{init}^3 produces an unsafe path along the sink edge. Quantitative results in Tab. 4 demonstrate that P_{init}^3 leads to worse video quality. The direct usage of videos generated with initial trajectory may cause unsafe behaviors in downstream

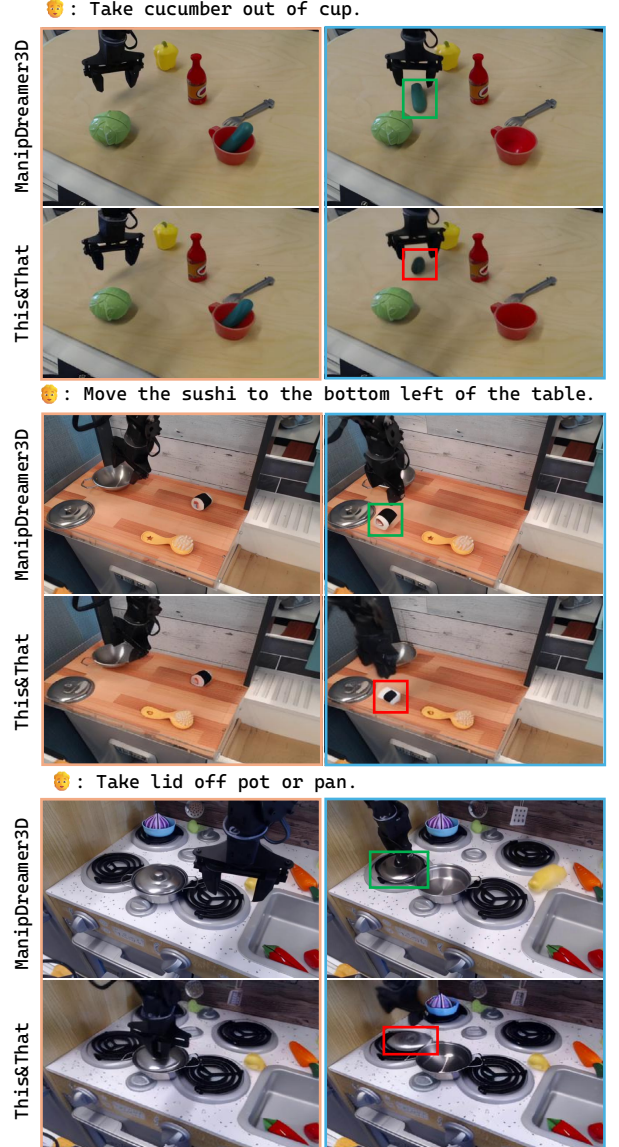


Figure 5: **Qualitative comparison between our ManipDreamer3D and This&That (both SVD-based).** Our method better preserves object appearance compared to This&That, which exhibits noticeable shape distortions in manipulation results.

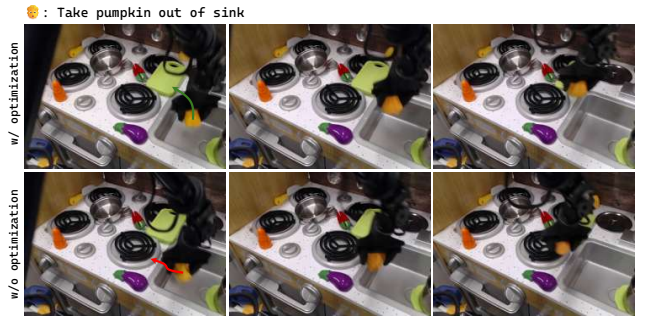


Figure 6: **Video visualization of path optimization effect.**

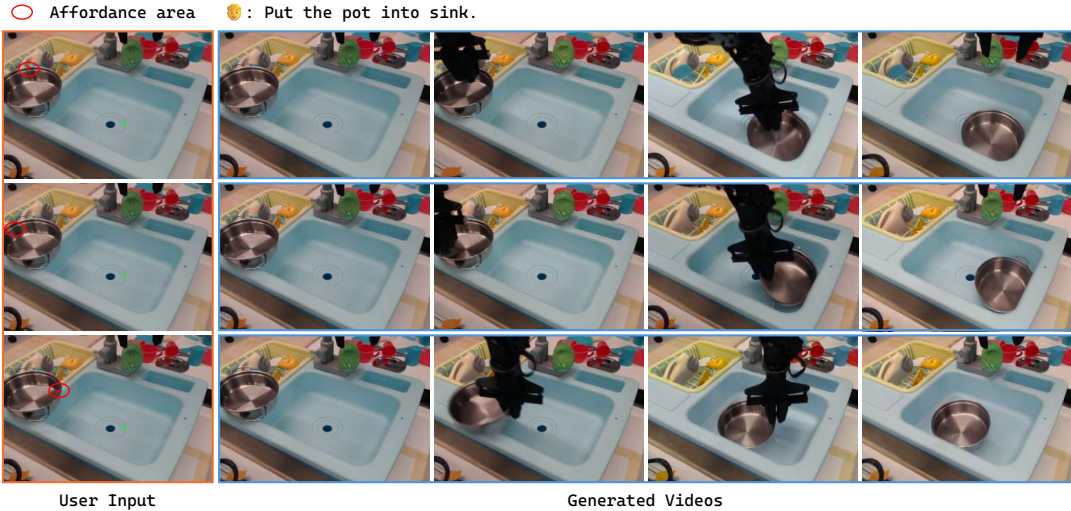


Figure 7: **Precision manipulation control demonstrations.** Our ManipDreamer3D exhibits fine-grained control capabilities by generating manipulation videos conditioned on specific object affordances.

Table 4: The video metric result of videos generated using the raw path and the optimized path.

Method	Aesthetic Quality \uparrow	Imaging Quality \uparrow	Temporal Flickering \uparrow	Motion Smoothness \uparrow	Subject Consistency \uparrow	background Consistency \uparrow
w/o trajectory optimization	53.29	66.03	96.93	97.81	95.13	96.07
w/ trajectory optimization	53.67	66.51	96.89	97.81	95.16	96.08

VLA applications, confirming the importance of trajectory optimization.

Precision Manipulation Control To evaluate the model’s capability in precision manipulation control, we conduct experiments using different functional parts (affordances) of objects to generate manipulation videos. The experiments employ our SVD-based model architecture to demonstrate fine-grained control over manipulation actions.

As illustrated in Fig. 7, we systematically vary the contact points on a pot object to test the model’s responsiveness to different manipulation conditions. The results show that our model successfully generates corresponding manipulation videos that accurately follow the specified affordance conditions, demonstrating its ability to handle intricate manipulation tasks.

Conclusion

We propose ManipDreamer3D , a framework for generating robotic manipulation videos guided by 3D occupancy-aware trajectories. First, we reconstruct the scene in 3D, then plan efficient end-effector and object trajectories, and finally synthesize a coherent video from the first-frame latent. This design enables comprehensive control at keypoint, full-trajectory, and affordance levels while requiring minimal manual annotation. Extensive experiments on diverse scenes demonstrate that ManipDreamer3D improves visual quality and spatial consistency, achieving stronger trajectory adherence compared with prior motion-controlled video generators.

Limitations and future work. Our current planning primarily targets rigid-body interactions and quasi-static grasps. Future work will explore more contact- and compliance-aware objectives, together with trajectory-conditioned generative priors that better capture articulation and deformation.

References

An, S.; Meng, Z.; Tang, C.; Zhou, Y.; Liu, T.; Ding, F.; Zhang, S.; Mu, Y.; Song, R.; Zhang, W.; et al. 2025. Dexterous manipulation through imitation learning: A survey. *arXiv preprint arXiv:2504.03515*.

Bai, J.; Bai, S.; Yang, S.; Wang, S.; Tan, S.; Wang, P.; Lin, J.; Zhou, C.; and Zhou, J. 2023. Qwen-VL: A Versatile Vision-Language Model for Understanding, Localization, Text Reading, and Beyond. *arXiv:2308.12966*.

Black, K.; Brown, N.; Driess, D.; Esmail, A.; Equi, M.; Finn, C.; Fusai, N.; Groom, L.; Hausman, K.; Ichter, B.; et al. 2024. π 0: A vision-language-action flow model for general robot control. *CoRR*, abs/2410.24164, 2024. doi: 10.48550. *arXiv preprint ARXIV.2410.24164*.

Blattmann, A.; Dockhorn, T.; Kulal, S.; Mendelevitch, D.; Kilian, M.; Lorenz, D.; Levi, Y.; English, Z.; Voleti, V.; Letts, A.; et al. 2023. Stable video diffusion: Scaling latent video diffusion models to large datasets. *arXiv preprint arXiv:2311.15127*.

Chen, J.; Lin, B.; Xu, R.; Chai, Z.; Liang, X.; and Wong, K.-Y. 2024. MapGPT: Map-Guided Prompting with Adaptive Path Planning for Vision-and-Language Navigation. In Ku, L.-W.; Martins, A.; and Srikanth, V., eds., *Proceedings of the 62nd Annual Meeting of the Association for Computational Linguistics (Volume 1: Long Papers)*, 9796–9810. Bangkok, Thailand: Association for Computational Linguistics.

Chen, Q.; Kiami, S. C.; Gupta, A.; and Kumar, V. 2023. GenAug: Retargeting behaviors to unseen situations via Generative Augmentation. In *Proceedings of Robotics: Science and Systems*. Daegu, Republic of Korea.

Ding, W.; Chen, B.; Xu, M.; and Zhao, D. 2020. Learning to collide: An adaptive safety-critical scenarios generating method. In *2020 IEEE/RSJ International Conference on Intelligent Robots and Systems (IROS)*, 2243–2250. IEEE.

Fang, Y.; Yang, Y.; Zhu, X.; Zheng, K.; Bertasius, G.; Szafrir, D.; and Ding, M. 2025. Reboot: Scaling robot learning with real-to-sim-to-real robotic video synthesis. *arXiv preprint arXiv:2503.14526*.

Fu, X.; Wang, X.; Liu, X.; Bai, J.; Xu, R.; Wan, P.; Zhang, D.; and Lin, D. 2025. Learning Video Generation for Robotic Manipulation with Collaborative Trajectory Control. *arXiv preprint arXiv:2506.01943*.

Gu, Z.; Yan, R.; Lu, J.; Li, P.; Dou, Z.; Si, C.; Dong, Z.; Liu, Q.; Lin, C.; Liu, Z.; et al. 2025. Diffusion as shader: 3d-aware video diffusion for versatile video generation control. In *Proceedings of the Special Interest Group on Computer Graphics and Interactive Techniques Conference Conference Papers*, 1–12.

Han, X.; Liu, M.; Chen, Y.; Yu, J.; Lyu, X.; Tian, Y.; Wang, B.; Zhang, W.; and Pang, J. 2025. Re³Sim: Generating High-Fidelity Simulation Data via 3D-Photorealistic Real-to-Sim for Robotic Manipulation. *arXiv preprint arXiv:2502.08645*.

Hanselmann, N.; Renz, K.; Chitta, K.; Bhattacharyya, A.; and Geiger, A. 2022. King: Generating safety-critical driving scenarios for robust imitation via kinematics gradients. In *European Conference on Computer Vision*, 335–352. Springer.

Hore, A.; and Ziou, D. 2010. Image quality metrics: PSNR vs. SSIM. In *2010 20th international conference on pattern recognition*, 2366–2369. IEEE.

Huang, J.; Gojcic, Z.; Atzmon, M.; Litany, O.; Fidler, S.; and Williams, F. 2023. Neural kernel surface reconstruction. In *Proceedings of the IEEE/CVF Conference on Computer Vision and Pattern Recognition*, 4369–4379.

Huang, N.; Wei, X.; Zheng, W.; An, P.; Lu, M.; Zhan, W.; Tomizuka, M.; Keutzer, K.; and Zhang, S. 2024a. S3Gaussian: Self-Supervised Street Gaussians for Autonomous Driving. *arXiv preprint arXiv:2405.20323*.

Huang, Z.; He, Y.; Yu, J.; Zhang, F.; Si, C.; Jiang, Y.; Zhang, Y.; Wu, T.; Jin, Q.; Champaisit, N.; et al. 2024b. Vbench: Comprehensive benchmark suite for video generative models. In *Proceedings of the IEEE/CVF Conference on Computer Vision and Pattern Recognition*, 21807–21818.

Kim, M. J.; Pertsch, K.; Karamcheti, S.; Xiao, T.; Balakrishna, A.; Nair, S.; Rafailov, R.; Foster, E.; Lam, G.; Sanketi, P.; et al. 2024. Openvla: An open-source vision-language-action model. *arXiv preprint arXiv:2406.09246*.

Kirillov, A.; Mintun, E.; Ravi, N.; Mao, H.; Rolland, C.; Gustafson, L.; Xiao, T.; Whitehead, S.; Berg, A. C.; Lo, W.-Y.; et al. 2023. Segment anything. In *Proceedings of the IEEE/CVF international conference on computer vision*, 4015–4026.

Li, Y.; Wei, X.; Chi, X.; Li, Y.; Zhao, Z.; Wang, H.; Ma, N.; Lu, M.; and Zhang, S. 2025. ManipDreamer: Boosting Robotic Manipulation World Model with Action Tree and Visual Guidance. *arXiv preprint arXiv:2504.16464*.

Ma, W.-D. K.; Lewis, J. P.; and Kleijn, W. B. 2024. Trailblazer: Trajectory control for diffusion-based video generation. In *SIGGRAPH Asia 2024 Conference Papers*, 1–11.

Mandi, Z.; Bharadhwaj, H.; Moens, V.; Song, S.; Rajeswaran, A.; and Kumar, V. 2022. Cacti: A framework for scalable multi-task multi-scene visual imitation learning. *arXiv preprint arXiv:2212.05711*.

Park, Y.; Bhatia, J. S.; Ankile, L.; and Agrawal, P. 2024. Dexhub and dart: Towards internet scale robot data collection. *arXiv preprint arXiv:2411.02214*.

Schmidt, L.; Santurkar, S.; Tsipras, D.; Talwar, K.; and Madry, A. 2018. Adversarially robust generalization requires more data. *Advances in neural information processing systems*, 31.

Unterthiner, T.; Van Steenkiste, S.; Kurach, K.; Marinier, R.; Michalski, M.; and Gelly, S. 2018. Towards accurate generative models of video: A new metric & challenges. *arXiv preprint arXiv:1812.01717*.

Wang, B.; Sridhar, N.; Feng, C.; Van der Merwe, M.; Fishman, A.; Fazeli, N.; and Park, J. J. 2025a. This&that: Language-gesture controlled video generation for robot planning. In *IEEE International Conference on Robotics & Automation (ICRA)*.

Wang, J.; Chen, M.; Karaev, N.; Vedaldi, A.; Rupprecht, C.; and Novotny, D. 2025b. Vggt: Visual geometry grounded transformer. In *Proceedings of the Computer Vision and Pattern Recognition Conference*, 5294–5306.

Wang, Z.; Bovik, A. C.; Sheikh, H. R.; and Simoncelli, E. P. 2004. Image quality assessment: from error visibility to structural similarity. *IEEE transactions on image processing*, 13(4): 600–612.

Wang, Z.; Li, M.; Wu, M.; Moens, M.-F.; and Tuytelaars, T. 2025c. Instruction-guided path planning with 3D semantic maps for vision-language navigation. *Neurocomputing*, 625: 129457.

Wang, Z.; Yuan, Z.; Wang, X.; Li, Y.; Chen, T.; Xia, M.; Luo, P.; and Shan, Y. 2024. Motionctrl: A unified and flexible motion controller for video generation. In *ACM SIGGRAPH 2024 Conference Papers*, 1–11.

Wei, X.; Wuwu, Q.; Zhao, Z.; Wu, Z.; Huang, N.; Lu, M.; Ma, N.; and Zhang, S. 2024. Emd: Explicit motion modeling for high-quality street gaussian splatting. *arXiv preprint arXiv:2411.15582*.

Wei, X.; Zhang, X.; Wang, H.; Wuwu, Q.; Lu, M.; Zheng, W.; and Zhang, S. 2025. OmniIndoor3D: Comprehensive Indoor 3D Reconstruction. *arXiv preprint arXiv:2505.20610*.

Wu, W.; Li, Z.; Gu, Y.; Zhao, R.; He, Y.; Zhang, D. J.; Shou, M. Z.; Li, Y.; Gao, T.; and Zhang, D. 2024. Draganything: Motion control for anything using entity representation. In *European Conference on Computer Vision*, 331–348. Springer.

Xu, H.; and Mannor, S. 2012. Robustness and generalization. *Machine learning*, 86(3): 391–423.

Yang, S.; Yu, W.; Zeng, J.; Lv, J.; Ren, K.; Lu, C.; Lin, D.; and Pang, J. 2025a. Novel demonstration generation with gaussian splatting enables robust one-shot manipulation. *arXiv preprint arXiv:2504.13175*.

Yang, X.; Li, B.; Xu, S.; Wang, N.; Ye, C.; Zhaoxi, C.; Qin, M.; Yikang, D.; Jin, X.; Zhao, H.; and Zhao, H. 2025b. ORV: 4D Occupancy-centric Robot Video Generation. *arXiv preprint arXiv:2506.03079*.

Yang, Z.; Teng, J.; Zheng, W.; Ding, M.; Huang, S.; Xu, J.; Yang, Y.; Hong, W.; Zhang, X.; Feng, G.; et al. 2024. Cogvideox: Text-to-video diffusion models with an expert transformer. *arXiv preprint arXiv:2408.06072*.

Yaseen, M. 2024. What is YOLOv8: An in-depth exploration of the internal features of the next-generation object detector. *arXiv* 2024. *arXiv preprint arXiv:2408.15857*.

Yin, S.; Wu, C.; Liang, J.; Shi, J.; Li, H.; Ming, G.; and Duan, N. 2023. Dragnuwa: Fine-grained control in video generation by integrating text, image, and trajectory. *arXiv preprint arXiv:2308.08089*.

Zhang, J.; Wang, K.; Wang, S.; Li, M.; Liu, H.; Wei, S.; Wang, Z.; Zhang, Z.; and Wang, H. 2024. Uni-navid: A video-based vision-language-action model for unifying embodied navigation tasks. *arXiv preprint arXiv:2412.06224*.

Zhou, G.; Hong, Y.; and Wu, Q. 2024. Navgpt: Explicit reasoning in vision-and-language navigation with large language models. In *Proceedings of the AAAI Conference on Artificial Intelligence*, volume 38, 7641–7649.

Zhou, S.; Du, Y.; Chen, J.; Li, Y.; Yeung, D.-Y.; and Gan, C. 2024. Robodreamer: Learning compositional world models for robot imagination. *arXiv preprint arXiv:2404.12377*.

Zitkovich, B.; Yu, T.; Xu, S.; Xu, P.; Xiao, T.; Xia, F.; Wu, J.; Wohlhart, P.; Welker, S.; Wahid, A.; Vuong, Q.; Vanhoucke, V.; Tran, H.; Soricut, R.; Singh, A.; Singh, J.; Sermanet, P.; Sanketi, P. R.; Salazar, G.; Ryoo, M. S.; Reymann, K.; Rao, K.; Pertsch, K.; Mordatch, I.; Michalewski, H.; Lu, Y.; Levine, S.; Lee, L.; Lee, T.-W. E.; Leal, I.; Kuang, Y.; Kalashnikov, D.; Julian, R.; Joshi, N. J.; Irpan, A.; Ichter, B.; Hsu, J.; Herzog, A.; Hausman, K.; Gopalakrishnan, K.; Fu, C.; Florence, P.; Finn, C.; Dubey, K. A.; Driess, D.; Ding, T.; Choromanski, K. M.; Chen, X.; Chebotar, Y.; Carbajal, J.; Brown, N.; Brohan, A.; Arenas, M. G.; and Han, K. 2023. RT-2: Vision-Language-Action Models Transfer Web Knowledge to Robotic Control. In Tan, J.; Toussaint, M.; and Darvish, K., eds., *Proceedings of The 7th Conference on Robot Learning*, volume 229 of *Proceedings of Machine Learning Research*, 2165–2183. PMLR.